IIETA International Information and Engineering Technology Association
Advancing the World of Information and Engineering

Journal Européen des Systèmes Automatisés
Vol. 59, No. 2, February, 2026, pp. 403-411
Journal homepage: http://iieta.org/journals/jesa

Cogging Torque Reduction of Line-Start Permanent Magnet Synchronous Motor with Skewed Stator

Le Anh Tuan[1], Nguyen Thi Lan[2], Do Nhu Y[3*]

[1] School of Electrical and Electronic Engineering, Hanoi University of Industry, Hanoi 100000, Vietnam
[2] FPT Polytechnic College, FPT University, Hanoi 100000, Vietnam
[3] Faculty of Electro–Mechanics, Hanoi University of Mining and Geology, Hanoi 100000, Vietnam

Corresponding Author Email: donhuy@humg.edu.vn

https://doi.org/10.18280/jesa.590210

Received: 1 November 2025
Revised: 25 January 2026
Accepted: 9 February 2026
Available online: 28 February 2026

Keywords:
line-start permanent magnet synchronous motor, permanent magnet, cogging torque, skewed stator, electric machine

ABSTRACT

Line-start permanent magnet synchronous motor (LSPMSM) has the advantages of high efficiency and the ability to self-start, making it a subject of research and application as a partial replacement for the widely used induction motors. However, LSPMSM also has significant drawbacks, and addressing these issues will help promote the motor. LSPMSM is difficult to start with and has high cogging torque (CT) during steady-state operation. CT causes undesirable effects such as mechanical vibrations, acoustic noise, and reduced efficiency. This paper studies the effectiveness of the skewed stator method in reducing CT. The paper applies the parametric analysis method and finite element methods to investigate different skewed angles of the stator. The subject of application is LSPMSM 2.2 kW, 2p = 4. The results show that with skew angles of 10° and 20°, the peak CT value is reduced nearly 50 times, and the electromagnetic torque ripple decreases by 6 times. Additionally, a skewed stator improves the starting quality and efficiency of the motor.

1. INTRODUCTION

According to statistics, global energy consumption is 30% for the industrial sector, 26% for transportation, and 22% for residential areas [1]. Energy consumption can be reduced through various solutions, such as using high-efficiency conversion devices [2], utilizing renewable energy sources [3], applying smart grid analysis, and developing and monitoring smart energy management systems [4]. Additionally, statistics show that electric motors typically account for about two-thirds of electricity consumption in the industrial sector of each country, equivalent to approximately 40% of total energy consumption [5]. Thus, applying high-efficiency electric motors to replace low-efficiency asynchronous motors that are commonly used in industries will be an effective solution in the strategy for energy conservation. Today, with the development of NdFeB rare earth magnet materials used in electric motors, line-start permanent magnet synchronous motors (LSPMSM) with high efficiency are considered a viable alternative to current motors [6, 7]. In terms of construction, LSPMSM combines features of induction motors (IM) and permanent magnet synchronous motors (PMSM). Therefore, LSPMSM has the advantages of both asynchronous motors and PMSM, including synchronous speed, low overall losses, high efficiency, and the ability to self-start. However, a major drawback of LSPMSM is not only its small starting torque [8] but also the typical issue of cogging torque (CT) during operation due to the use of permanent magnets (PMs) [9, 10]. Consequently, many studies have focused on reducing CT to help promote the use of PMSMs in applications requiring high-efficiency electric motors [11].

LSPMSM is constructed with squirrel cage bars on the rotor, which can be attached to the surface or embedded. Thus, like PMSM, LSPMSM experiences CT during operation. The CT in motors using PMs is generated by the interaction between the PMs mounted on the rotor and the slots on the stator. CT is an unwanted torque component as it adversely affects the operation of the motor. CT reduces the quality of the torque because it generates mechanical vibrations and acoustic noise [12]. Therefore, there are currently many studies aimed at mitigating this torque for motors using PMs. Studies to limit CT can be categorized into two methods: control and motor design. Control methods to reduce the CT in motors using PMs can be listed as follows: Sumega et al. [13] investigated two different methods to determine the CT of three-phase PMSM. Based on the results from the two methods, a CT map was constructed and subsequently applied in a Field-Oriented Control (FOC) algorithm to minimize ripple in speed and electromagnetic torque (ET) of the motor. Pierpaolo and Saponara [14] proposed a sensorless control method based on an Extended Kalman Filter observer and a linear feedback control system. The results indicated that even without a sensor, the proposed control solution could still minimize CT. Petro et al. [15] researched a method for injecting high-frequency (HF) signals to accurately estimate the rotor position of PMSMs. Their proposed method improved control quality by reducing the signal injection time and compensating for CT, thereby minimizing current and speed ripple. Chu et al. [16] examined the speed control of

Brushless DC motors (BLDC). This paper proposed using a three-step nonlinear controller based on a new observer to enhance performance by mitigating CT at low speeds. The results showed that the errors caused by CT regarding the system were significantly reduced at low speeds. Liu et al. [17] investigated the Iterative Learning Control (ILC) method, alongside the conventional proportional and integral (PI) controller (i.e., PI-ILC), as a method to minimize CT. Experimental results demonstrated that the proposed improved ILC method showed enhanced performance, with oscillations due to cogging torque minimized.

In addition to applying control methods to limit cogging torque, the method of modifying the design is more commonly used. The popular design methods to reduce CT can be summarized as follows [18]: Flux barrier, PM design, stator dummy and rotor notches, slot opening, and skewing. Kim [19] proposed a method to minimize CT in Inserted PMSMs (IPMSM) by applying an asymmetric flux barrier design and inverting lamination. The research results showed that an asymmetric flux barrier design in the rotor of the PMSM could achieve good results without needing to skew the PMs. Simón-Sempere et al. [20] investigated a new method to reduce CT in axial flux permanent magnet motors (AFPM) based on the shape of the PMs. The results indicated that the proposed method is accurate, unique, and quick to compute without needing to use finite element methods (FEM). Anuja et al. [21] researched and proposed a new method to minimize CT based on the uneven positioning of the PMs. The results indicated that CT in the analysis decreased, and comparisons with the FEM method demonstrated the effectiveness of the proposed method. Nakano et al. [22] proposed a new stator core structure to minimize cogging torque caused by tolerances in the manufacturing of PMSM. The research results showed that by applying a configuration containing dummy slots, CT could be very effectively minimized. Xia et al. [23] studied and confirmed that the auxiliary slot method is an effective approach to minimize CT in PMSM. The analysis results showed that with deeper auxiliary slots, the peak CT changed significantly in the initial phase and then stabilized. Hwang et al. [24] researched an improved mechanical method to reduce CT and torque ripple (TR). In this study, a method was proposed to reduce vibration and noise mechanically by designing a notched rotor shape. Morimoto et al. [25] proposed a design method to create notches on the surface of the rotor to reduce CT in IPMSM with dual-layer PMs. The FEA showed that the CT in the model with optimized notch positions was significantly reduced. Zhao et al. [26] proposed a stepped slot-opening shift method to reduce CT in IPMSM. The research results indicated that this method could achieve CT reduction like the skewing slots method while maintaining the three-phase symmetry of the motor. Patel [27] studied and presented a gap shifting technique to reduce CT for axial flux BLDCs suitable for two-wheeled electric vehicle applications. The research results demonstrated that the gap shifting technique was effective in reducing CT in axial flux BLDCs, with CT decreasing from 1.23 Nm to 0.63 Nm. Moreover, the skewing method is widely applied to reduce CT, and there are two ways for skewing: skewing the stator and rotor. Jiang et al. [28] studied the effects of different skewed rotor patterns on CT and torque ripple, average torque, and axial force in IPMSMs. A genetic algorithm was used to minimize CT. The results showed that linear skewed rotor patterns reduced CT but increased axial force. Hao et al. [29] studied three stepped skewed stator structures, including three-step skewed stator, two-step skewed stator, and improved two-step skewed stator to enhance CT in Linear Flux Switching PMSM (LFSPM). Based on FEA, suitable skew angles were selected based on the largest difference in CT reduction rate.

Thus, to reduce CT, the methods of skewed stator and rotor are commonly applied in design. This method is not only easy to implement in manufacturing but also has proven effective in reducing CT. Therefore, this paper applies this method to study the reduction of CT for LPSMSMs.

In summary, motors using PMs have the drawback of high CT during operation. CT causes mechanical vibrations and acoustic noise, reducing the efficiency of the motor. Since LSPMSM is a motor that uses PMs, it also experiences CT, making research to mitigate this drawback a measure to promote the motor. The most common methods to reduce CT in PMSMs are skewing the stator and rotor. This method has proven effective and is easy to implement during the manufacturing of the motor. Although skewing is widely used in PMSMs, its application in LSPMSMs-especially with continuous skew type remains underexplored. Therefore, this paper will investigate the application of the skewed stator method to reduce CT. The research results of this paper will be applied to LPSMSM 2.2 kW, 2p = 4. Based on the research findings, the most effective and appropriate skew angle will be proposed for the fabrication of LPSMSM 2.2 kW, 2p = 4.

2. ANALYTICAL ANALYSIS OF COGGING TORQUE AND THE EFFECT OF SKEWED STATOR METHOD ON COGGING TORQUE

2.1 Cogging torque of permanent magnet motors

The basic operation of a synchronous electric motor is based on the electromagnetic interaction between the rotor's excitation magnetic field and the magnetic field generated by the current in the stator windings. In the case of PMSM, even when the motor is not powered, and no current flows through the stator, there still exists an interaction force between the rotor's PMs and the stator teeth. This magnetic interaction force depends on the magnetic flux density or the field strength in the air gap (AG) and varies according to the relative position between the rotor and stator. This variation creates an uneven torque, known as “cogging torque” [30].

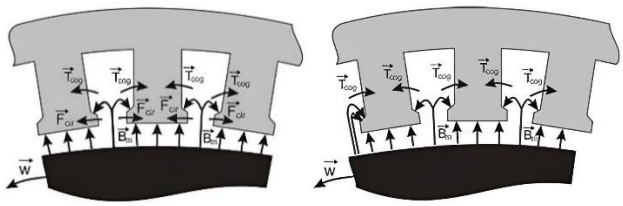

(a) Alignment (b) Non-aligned

Figure 1. The relative position between the permanent magnet (PM) and the stator teeth generates cogging torque

The machine with slots makes the stator anisotropic, creating a transformation of magnetic energy in the AG. This transformation generates a circumferential attraction force (F_{cir}) aimed at minimizing the system's energy, aligning the center of the PM with the center of the stator teeth or slots. Each component of the force F_{cir} generates a CT component, as illustrated in Figure 1 [30]. It can be observed that this alignment will cancel out the CT components, resulting in a

total CT of zero as in Figure 1(a). Therefore, this alignment position is considered magnetically stable.

Figure 1(b) shows an unstable magnetic position when the PMs and stator slots are not aligned. The total CT is non-zero, leading to a tendency for the PMs to move toward a stable position. The LSPMSM is modeled by two interacting components: the PM and the winding. The energy is generated by three factors: the self-inductance energy of the winding, the magnetic energy, and the mutual inductance energy between the winding and the PM. The ET is derived from the total magnetic energy W or the total equivalent energy W_c, as a function of the mechanical angle [30].

$$W_c = \frac{1}{2}Li^2 + \frac{1}{2}(R + R_m)\phi_m^2 + Ni\phi_m \tag{1}$$

where, R and R_m are the reluctance of the magnetic circuit and the reluctance of the PM, L is the inductance of the winding, ϕ_m is the magnetic flux linked through the winding created by the permanent magnet, N is the number of turns in the winding, and i is the current flowing through the winding. The ET is determined by:

$$T = \frac{\partial W_c}{\partial \theta} \tag{2}$$

$$T = \frac{1}{2}i^2\frac{dL}{d\theta} - \frac{1}{2}\phi_m^2\frac{dR}{d\theta} + \mathrm{Ni}\frac{d\phi_m}{d\theta} \tag{3}$$

Since the inductance L of the winding is a constant, in the absence of excitation current ($i = 0$), only the second term will appear in Eq. (1). Additionally, the reluctance of the PM and ϕ_m are also constants. Therefore, the CT can be estimated by focusing on the magnetic field interaction as well as the variation of the magnetic circuit reluctance between the winding and the PM according to the relative angle between the PM and the stator teeth, leading to:

$$T_{cogging} = \frac{\partial W_c}{\partial \theta}_{i=0} = -\frac{1}{2}\phi_m^2\frac{\partial R}{\partial \theta} \tag{4}$$

The stages of the CT pulse cycle are shown in Figure 2, and the variation of CT with respect to mechanical angle positions is depicted in Figure 3 [31].

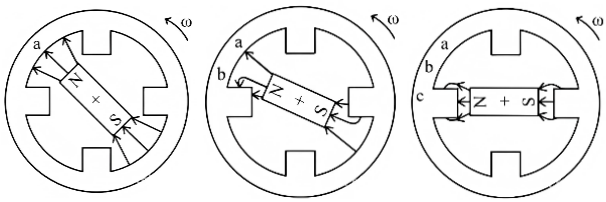

Figure 2. Relative position of permanent magnet (PM) and stator

The CT graph generated at relative positions as shown in Figure 2, corresponds to Figure 3.

Figures 2 and 3 show that CT depends on the position of the stator teeth relative to the PM. The magnetic field generated by the PM tends to seek a position with the lowest reluctance. The shape of the CT in PM motors depends on the arrangement of the PMs and the stator teeth. The period of the CT pulse cycle is influenced by the geometric structure of the electric machine. CT reduces the quality of the ET and affects the smooth operation of the machine, causing mechanical vibrations and acoustic noise. Therefore, in practice, methods are researched in design and control to reduce CT.

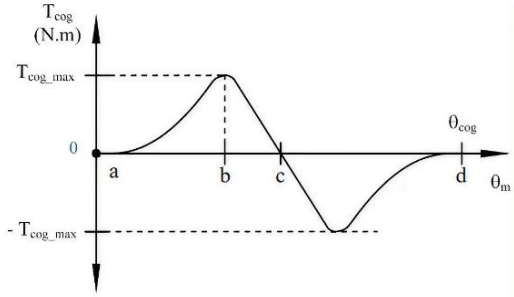

Figure 3. The cogging torque (CT) with respect to the relative position of the permanent magnet (PM) and stator

2.2 The effect of skewed stator

In operation, it is desired for CT to be as small as possible. It must be mathematically represented to analytically eliminate CT. First, the angle θ_{cog} of one cycle of CT can be expressed by the equation [32]:

$$\theta_{cog} = \frac{360^0}{LCM(N_p, N_s)} \tag{5}$$

where, N_p and N_s are the number of poles and the number of stator slots, respectively, $LCM(N_p, N_s)$ is the least common multiple of N_p and N_s. Therefore, the period of CT depends on the number of poles and slots, with a larger $LCM(N_p, N_s)$ resulting in a shorter period. As a result, the larger the $LCM(N_p, N_s)$, the smaller the amplitude of the CT.

CT with respect to the mechanical angle is represented in Figure 3, assuming no consideration of the skew, as defined by the equation [32]:

$$\begin{aligned} T(\theta_m) &= \frac{\pi L_{Fe}.LCM(N_p, N_s)}{4\mu_o}\left(R_2^2 - R_1^2\right) \\ &\times \sum_{n=1}^{\infty} nG_{ak}B_{am}\sin\left(n\theta_m \times LCM(N_p, N_s)\right) \end{aligned} \tag{6}$$

where, L_{Fe} is the length of the core, R_1, R_2 are the inner and outer radii of the AG, respectively. G_{ak}, B_{am} are coefficients related to the relative permeability and magnetic flux density of the AG. If a step skew is implemented with each step being M, when considering the skew, the CT can be determined by the equation:

$$\begin{aligned} T(\theta_m) &= \frac{\pi L_{Fe}.LCM(N_p, N_s)}{4\mu_o M}\left(R_2^2 - R_1^2\right) \\ &\times \sum_{n=1}^{\infty} nG_{ak}B_{am}\frac{\sin\dfrac{n\theta_{skew}.LCM(N_p, N_s)}{2}\dfrac{M}{M-1}}{\sin\dfrac{n\theta_{skew.step}.LCM(N_p, N_s)}{2}} \\ &\times \sin\left[n\left(\theta_m + \frac{\theta_{skew.step}}{2}\right).LCM(N_p, N_s)\right] \end{aligned} \tag{7}$$

where, $\theta_{skew.step}$ is the skew angle for each step. To minimize CT, the condition is $T_{cog} = 0$, and the conditions to achieve this are:

$$\sin\frac{n\theta_{skew}LCM\left(N_p,N_s\right)}{2}\frac{M}{M-1}=0 \tag{8}$$

The value θ_{skew} that satisfies the condition of Eq. (8) is determined:

$$\theta_{skew}=\frac{M-1}{M}\frac{360^{\circ}}{LCM\left(N_p,N_s\right)} \tag{9}$$

Thus, from Eqs. (8) and (9), it can be observed that CT in motors using PMs can be reduced by appropriately selecting the skew angle θ_{skew} of the rotor or stator core. In this paper, the evaluation for selecting the appropriate θ_{skew} for the experimental LSPMSM is conducted through simulations using the FEA on Ansys/Maxwell software. In Chapter 3 below, simulations will be conducted to evaluate the effect of the skew angle θ_{skew} on the starting characteristics (speed) of the LSPMSM. From these results, the theoretical and simulation compatibility will be demonstrated. Additionally, other important characteristics of the motor will also be investigated.

3. SIMULATION OF LSPMSM CONSIDERING SKEWED STATOR

The paper studies the effect of the skewed stator on CT. The type of the skewed stator considered in the simulation is continuous type due to the commonality of the method [32], when $M\rightarrow\infty$, Eq. (9) transforms into Eq. (5). The LSPMSM has the number of stator slots with $N_s = 36$, so $\theta_{skew} = 10°$.

This paper will investigate skew angles corresponding to a skew of 2 steps, specifically 20°, to validate the correctness of the theory and assess the variation of CT when skewing the stator. This is fully aligned with the literature [33, 34]. Therefore, in the simulation scenario, the skew step θ_{skew} is varied in the simulation from 0 to 2 slots (corresponding to 20°). Each simulation step corresponds to 5°. Based on the results obtained, the characteristics of the motor will be analyzed and evaluated. Some skew angles in the simulation scenario are illustrated in Figures 4(a) and (b).

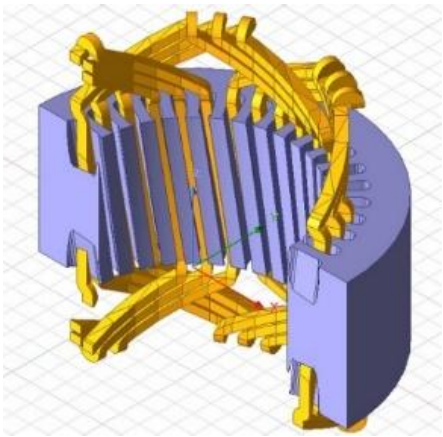

(a) Continuous type of skewed stator

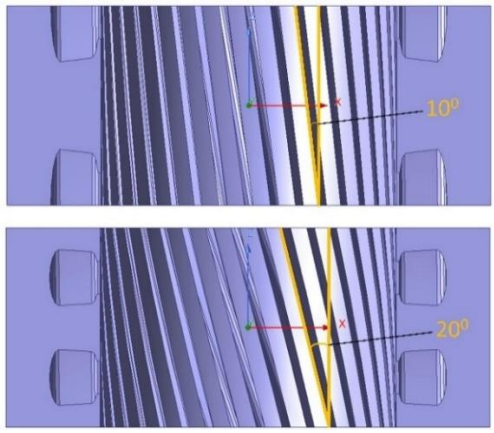

(b) Continuous type of skewed stator with 10° and 20° angle

Figure 4. Skewed stator of line-start permanent magnet synchronous motors (LSPMSM)

3.1 Speed characteristics

The speed characteristic is commonly used to evaluate the starting capability of LSPMSM. Since LSPMSM has the drawback of being difficult to start, this characteristic needs to be addressed. In the simulation, the load applied to the motor shaft is equal to the rated load. The startup speed characteristic of the 2.2 kW LSPMSM with different stator skew angles is shown in Figure 5.

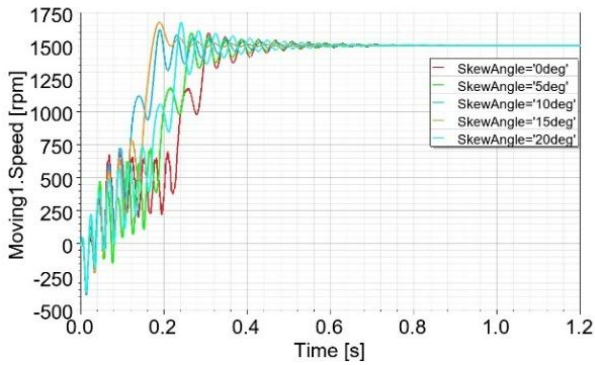

Figure 5. Speed characteristics of line-start permanent magnet synchronous motors (LSPMSM)

Thus, with different stator skew angles, the LSPMSM can start successfully. The speed characteristic goes through several "dip" phases before the motor can reach synchronous speed. Table 1 summarizes the starting quality of the LSPMSM.

Table 1. Parameters for evaluating the speed characteristics

Skew Angle	Number of Dips	Transient Time t_{ts} (ms)	Settling Time t_{st} (ms)
0°	10	300	980
5°	9	259	922
10°	8	183	841
15°	6	173	622
20°	8	233	880

With each different stator skew angle, the performance curve of the motor also varies. Moreover, it can be noted that without skewing, the motor has the most difficulty starting. In this case, to reach maximum speed initially, it must pass

through 10 speed dips. After approximately 1 second, the motor achieves stable synchronous speed. Furthermore, the investigation indicates that at a skew angle of 15°, the startup is the easiest. In this scenario, the motor passes through 6 dips to reach maximum speed first, and after about 0.6 seconds, the motor reaches stable synchronous speed.

3.2 Current characteristics

In addition to the speed characteristics, the current characteristics are also studied. Through the current characteristics, the maximum starting current can be examined to implement measures to mitigate the effects of this surge current. Furthermore, the current during the steady state time is also investigated to evaluate the magnitude of the current under rated operating conditions. The simulated current characteristics are shown in Figure 6.

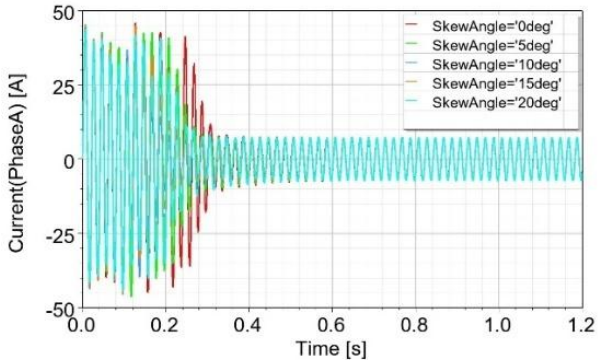

Figure 6. Current characteristics of line-start permanent magnet synchronous motors (LSPMSM)

The LSPMSM starts with a relatively high current. The duration of the starting current will vary depending on the skew angle. In the case of no skewing, the duration of the current maintained during startup with a high amplitude is longer. Thus, in some cases, this can lead to significant overheating of the motor. However, the peak current amplitude during startup is the same across cases, reaching approximately 45 A (about 6 times the amplitude of the rated current).

3.3 Back electromotive force characteristics

In addition to the two aforementioned characteristics, the back-EMF characteristic is also considered. The back-EMF characteristic reflects the magnetic flux generated by the magnetic field of the PM in the stator windings. Furthermore, this characteristic is influenced by the path of the anisotropic magnetic field due to the structure of the stator teeth and rotor. The simulated back-EMF characteristic is shown in Figure 7.

The back-EMF characteristic obtained in Figure 7 during the simulation has a non-sinusoidal shape. However, the back-EMF waveform contains dips and varies periodically with the supply frequency in the cases of skewing angles of 0°, 5°, and 15°. In contrast, for the cases of skewing at 10° and 20°, although the waveform exhibits some ripples, the characteristics of these two cases are closer to a sine wave. To assess the degree of non-sinusoidal behavior of the periodic waveform of the back-EMF characteristic obtained during the simulation, Fast Fourier transform (FFT) analysis was employed to analyze the back-EMF waveform. The results of the FFT analysis of the back-EMF waveform for the skewed stator cases are shown in Figure 8.

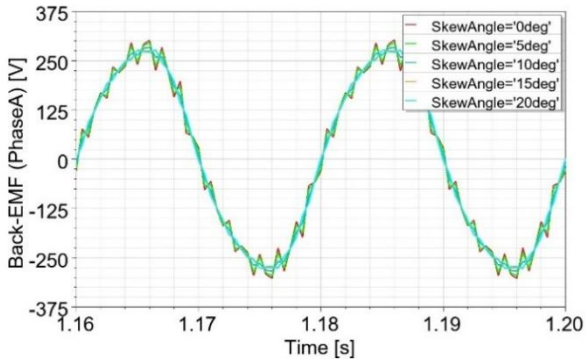

Figure 7. Back-EMF characteristics of line-start permanent magnet synchronous motors (LSPMSM)

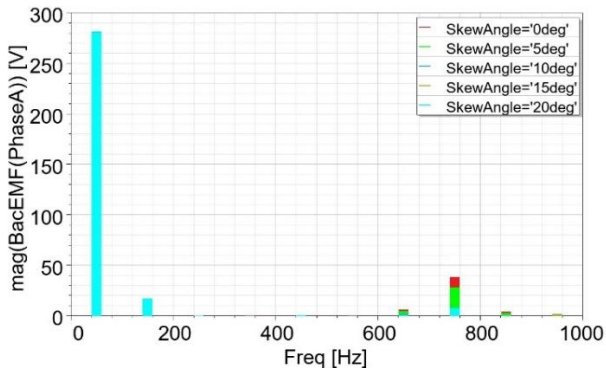

Figure 8. Fast Fourier transform (FFT) analysis of the simulated back-EMF waveform

The back-EMF waveform of the LSPMSM, when analyzed using FFT, shows the presence of multiple harmonic components. Due to the periodic and symmetrical nature of the back-EMF waveform over one cycle, only odd-order harmonic components are present in the FFT analysis. Among the harmonics, the 15th harmonic has a significant amplitude, followed by the 3rd harmonic. Additionally, for the skew angles of 0°, 5°, and 15°, the 15th harmonic has a large amplitude. In contrast, the 10° and 20° skew angles exhibit larger amplitudes at the 3rd harmonic. However, compared to the 15th harmonic, the amplitude of the 3rd harmonic in all skew angle cases is much smaller. The amplitude values of each harmonic for different skew angles are summarized in Table 2. Furthermore, to assess the distortion of the waveform, the $\Delta E\%$ is used to assess the degree of deviation of the fundamental back-EMF waveform (the 1st order) from the value of the voltage of power supply [8].

$$\Delta E\% = \left| \frac{E_{1NB} - 220}{E_{1NB}} . 100\% \right| \quad (10)$$

Table 2. Fast Fourier transform **(**FFT) analysis of the harmonic components of the back-EMF

Skew Angle	1st	3rd	13th	15th	THD	$\Delta E\%$
0°	281.3	14	6.5	38.3	14.7	10.6
5°	281.3	14.3	5	28.6	11.5	10.6
10°	281.2	15.2	1.9	8.3	6.2	10.6
15°	281	16.2	0.5	6.5	6.8	10.7
20°	280.6	17.3	1.1	7.8	6.2	10.8

From Table 2, the amplitude of the 1st harmonic is approximately equivalent across all cases, with negligible differences. The deviation of the 1st harmonic back-EMF waveform from the rated fundamental voltage of the line *ΔE%* is approximately 10.6% in all examined cases. The THD index is used to assess the distortion of the sinusoidal waveform; the higher this index, the greater the harmonic distortion. Higher-order harmonics can cause unwanted effects such as losses, vibrations, and noise. Thus, for skew angles of 5° and 10°, the THD index is at its lowest, indicating that the back-EMF waveform of the LSPMSM is closer to a sine wave. Additionally, the *ΔE%* index reflects the deviation between the fundamental back-EMF waveform value and the supplied voltage. The back-EMF value is the excitation source of the machine, which affects all operational parameters of the motor. Typically, it is designed to be sufficiently excited in the steady state. Therefore, in Table 1, with equivalent *ΔE%* values and a deviation from the supplied voltage of 10.6%, the motor is adequately excited. However, with different deviations, the harmonic indices of these waveforms vary.

3.4 Cogging torque characteristics

The simulated CT characteristics are shown in Figure 9 below to evaluate the effectiveness of the skew. The simulation scenario is studied for the experimental LSPMSM, utilizing a parametric analysis method.

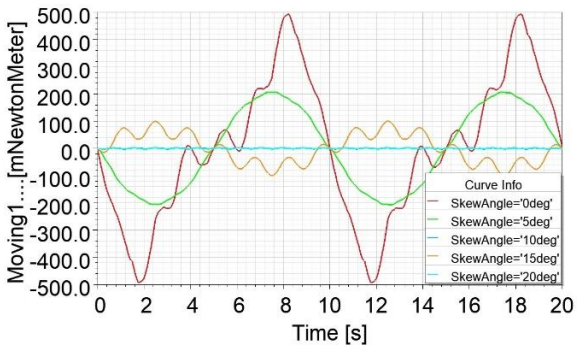

Figure 9. Cogging torque waveforms

The cogging torque waveform is periodic with a cycle matching the frequency of the power supply, as shown in Figure 9. The skew angle significantly influences the shape of the CT waveform. Additionally, the simulation results demonstrate the effectiveness of the skewing method in reducing CT. When the stator is not skewed, the amplitude of the CT reaches its maximum value at $T_{cog.max}$ = 492 mNm. Meanwhile, with skew angles of 10° and 20°, the CT characteristics are similar. Furthermore, with skew angles of 10° and 20°, the amplitude of CT decreases significantly, with $T_{cog.max}$ = 492 mNm. The summary of $T_{cog.max}$ for each skew angle is presented in Table 3 below.

Table 3. $T_{cog.max}$ with different skew angles

Skewing Angle	$T_{cog.max}$ (mNm)
0°	492
5°	206
10°	10
15°	100
20°	10

From Table 3, the effectiveness of appropriately choosing the skew angle concerning CT can be observed. If the skew of the stator is selected as 1 or 2 slots, corresponding to 10° and 20°, the amplitude $T_{cog.max}$ simulated for the experimental LSPMSM reduces by nearly 50 times.

The CT waveform of the LSPMSM is periodic with the cycle of the power supply. The CT waveforms are subjected to FFT analysis to evaluate and analyze the harmonic components. The results of the harmonic component analysis of CT waveforms are shown in Figure 10.

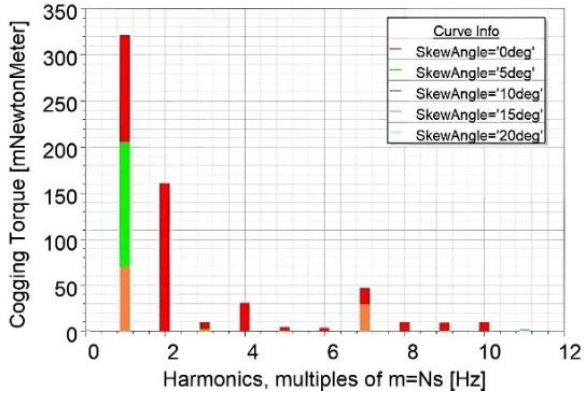

Figure 10. Fast Fourier transform (FFT) analysis of the cogging torque (CT) waveforms

When performing the FFT analysis, it can be observed that the CT waveform contains harmonic components with both odd and even orders. This is due to the waveform being periodic but asymmetrical over half a cycle. This result demonstrates the consistency of the simulation with Eq. (7), as the CT characteristics contain harmonic components of varying orders.

3.4 Electromagnetic torque characteristics

CT is the parasitic torque of PM motors. This torque contributes to generating fluctuations in the operating torque. Therefore, for measures to mitigate CT, in addition to the CT characteristics, the ET characteristics must also be considered. The ET of the LSPMSM with various stator skew angles is simulated as shown in Figure 11.

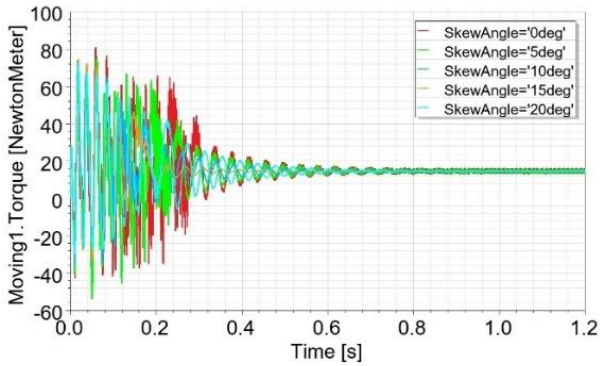

Figure 11. ET characteristics of line-start permanent magnet synchronous motors (LSPMSM)

Similar to the current characteristics, the LSPMSM starts with a relatively high starting torque. In the case of no skewing, the time for the ET to reach steady state is longer.

Additionally, in the steady state, the ET of the motor is not stable at the rated value (14.4 Nm) but fluctuates around this rated value with significant amplitude.

In the steady-state mode, this level of fluctuation is desired to be as small as possible. The cause of this torque ripple is partly due to the CT [9]. Additionally, the coefficient *k* is used to evaluate the level of this fluctuation [35]. The coefficient *k* is defined:

$$k = \frac{T_{\max} - T_{\min}}{T_{avg}} \tag{11}$$

where, T_{max}, T_{min} represent the maximum and minimum value of the instantaneous torque, respectively, T_{avg} is the average value of the torque. The coefficient *k* is calculated and summarized as shown in Table 4.

Table 4. Coefficient *k* of line-start permanent magnet synchronous motors (LSPMSM)

Skewing Angle	T_{max} (Nm)	T_{min} (Nm)	Coefficient *k*
0°	16.27	13.05	0.23
5°	15.95	13.35	0.19
10°	14.93	14.04	0.06
15°	15.87	13.98	0.14
20°	15.04	14.19	0.06

Thus, when operating in the steady state with skew angles of 10° and 20°, the ripple of the ET is minimized, with the corresponding coefficient *k* equal to 0.06. Thus, these results are entirely consistent with the analytical theory presented in Figures 2 and 3, as well as Eqs. (9) and (10). Therefore, to minimize CT, the stator can be skewed by an angle that is a multiple of one tooth, with the simplest approach being to skew one tooth of the stator.

The maximum ripple occurs when the stator is not skewed, at which point the coefficient *k* equals 0.23, resulting in a reduction of the ripple by a factor of 6. It is evident that CT is one of the main causes of torque ripple in the steady-state operation of the motor. This level of ripple is effectively minimized using the method of skewed stator.

3.5 Efficiency characteristics

The efficiency of the LSPMSM is confirmed to be high. Therefore, the efficiency characteristics of the LSPMSM are also examined in this paper. The working efficiency of the LSPMSM is the ratio of mechanical power to the electrical power consumed. The efficiency characteristics are simulated as shown in Figure 12.

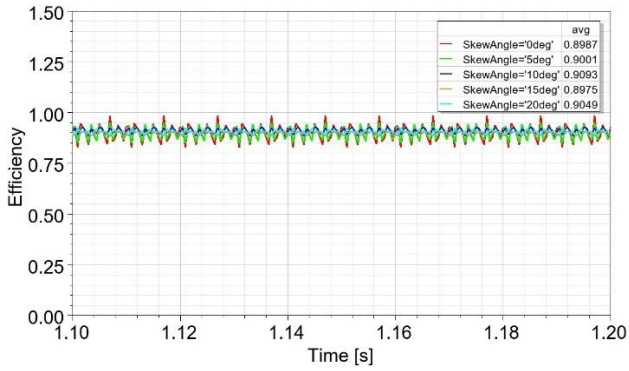

Figure 12. Efficiency of line-start permanent magnet synchronous motors (LSPMSM) in steady state

The LSPMSM in all cases within the simulation scenario exhibits an efficiency rating of IE4 (≥ 89.5%). Thus, the efficiency characteristics of the motor are also influenced by the skew angle. However, the variation in efficiency between the cases is not significant. The case with the lowest efficiency occurs when the stator is not skewed. The two skewed cases at 10° and 20° exhibit the highest efficiency in steady-state time. Therefore, it is evident that CT also has a detrimental effect on the operating efficiency of the motor.

4. EXPERIMENTAL RESULTS

A LSPMSM 2.2 kW, 2p = 4 was fabricated for experimentation. The experimental LSPMSM has a stator and rotor configuration with dimensions for teeth, slots, PM slot sizes, PM materials, etc., similar to those used in the simulation. However, due to manufacturing difficulties, the authors only experimented with no skewed stator slots. The experimental model is shown in Figure 13.

In the experimental model, the ZHKY901 torque sensor is used to measure the torque value. In the experiment, the ZHKY901 is connected coaxially with the experimental LSPMSM and the load. During the experiment, with no load, the shaft is rotated to measure the value of CT. The maximum experimental CT value obtained will be compared with the results obtained from the simulation shown in Figure 9. Experimental and simulation results of the maximum cogging torque value are presented in Table 5.

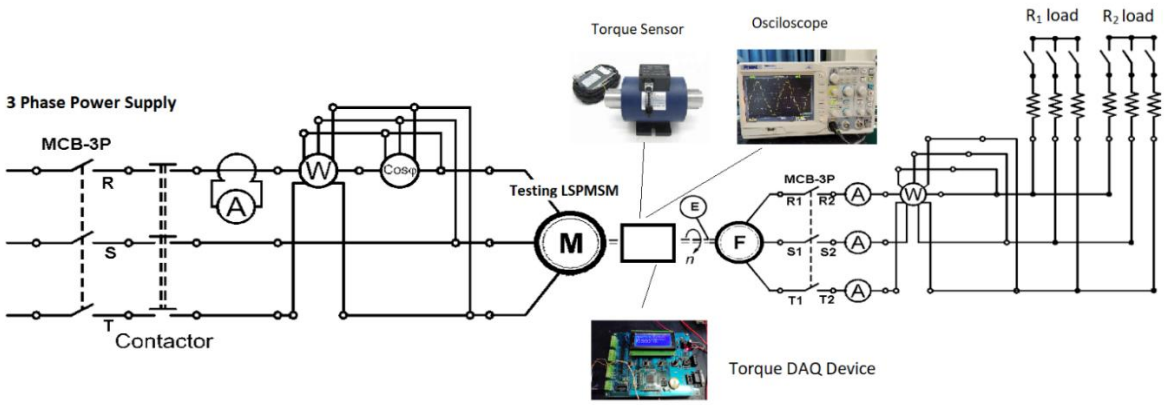

Figure 13. Experimental diagram of the line-start permanent magnet synchronous motors (LSPMSM) 2.2 kW, 2p = 4

Table 5. The maximum cogging torque value

Testing (mNm)	Simulation (mNm)	Error (%)
485	492	1.5

Table 5 shows that the results are consistent between the experiment and the simulation. The error between the experimental and simulated results is approximately 1.5%. Thus, the experimental results indicate that in the case of non-skewed stator, the experimental and simulated outcomes are similar, with the actual error between the two methods being negligible. This result demonstrates the accuracy of the FEM software in simulations, confirming that it is a very effective tool for validating designs. Additionally, this result also affirms the accuracy of the simulation results with respect to other skewing angles of stator slot.

5. CONCLUSIONS

The LSPMSMs is a high-efficiency motor that can meet increasingly stringent standards for electric motors. With this advantage, the motor can be used to replace the currently popular IMs. However, the motor has some shortcomings that need to be addressed, such as difficulties in starting and CT during steady-state operation. Overcoming these shortcomings from the design stage will contribute to the widespread adoption of this motor.

In this paper, a study is conducted on the impact of skewed stator method on reducing CT. The subject of the study is LSPMSM 2.2 kW, 2p = 4, N_s = 36. The parametric analysis method and FEA software are proposed for evaluation in simulations. The research results indicate a significant effectiveness in reducing CT when appropriately selecting the skew angle of the stator. With the skewing angles that are a multiple of one stator tooth, specifically 10° and 20°, there is an equivalent reduction in CT, with the peak amplitude of CT decreasing nearly 50 times compared to non-skewed. Additionally, skewed stator improves the motor's startup characteristics, resulting in faster startup times. The torque ripple is also significantly reduced, with reductions of 6 times observed at skew angles of 10° and 20% compared to non-skewed. In terms of efficiency, the skew angles of 10° and 20° also yield the highest efficiency; however, the difference in efficiency levels is minimal. From these results, it can be concluded that the method of skewed stator should be applied in the manufacturing of LSPMSM due to its feasibility and effectiveness in mitigating CT and torque ripple - two significant drawbacks of LSPMSM.

REFERENCES

[1] Farghali, M., Osman, A.I., Mohamed, I.M., Chen, Z., Chen, L., Ihara, I., Yap, P.S., Rooney, D.W. (2023). Strategies to save energy in the context of the energy crisis: A review. Environmental Chemistry Letters, 21(4): 2003-2039. https://doi.org/10.1007/s10311-023-01591-5

[2] Le Anh, T., Bien, T.T., Xuan, C.N., Do Anh, T., Do Nhu, Y. (2024). Analysis of permanent magnet demagnetization during the starting process of a line-start permanent magnet synchronous motor. Engineering, Technology & Applied Science Research, 14(6): 17900-17905. https://doi.org/10.48084/etasr.8576

[3] Sang, L.Q., Li, Q.A., Maeda, T., Kamada, Y., Huu, D.N., Tran, Q.T., Sanseverino, E.R. (2023). Study method of pitch-angle control on load and the performance of a floating offshore wind turbine by experiments. Energies, 16(6): 2762. https://doi.org/10.3390/en16062762

[4] Selvaraj, R., Kuthadi, V.M., Baskar, S. (2023). Smart building energy management and monitoring system based on artificial intelligence in smart city. Sustainable Energy Technologies and Assessments, 56: 103090. https://doi.org/10.1016/j.seta.2023.103090

[5] Saidur, R. (2010). A review on electrical motors energy use and energy savings. Renewable and Sustainable Energy Reviews, 14(3): 877-898. https://doi.org/10.1016/j.rser.2009.10.018

[6] Tran, D.K., Le, A.T., Do, N.Y., Do, A.T. (2025). Impact of temperature on the operating characteristics of line-start permanent magnet synchronous motors. Journal Européen des Systèmes Automatisés, 58(9): 1921-1930. https://doi.org/10.18280/jesa.580914

[7] Le Anh, T., Trong, C.T., Duc, C.Q., Do Nhu, Y. (2024). Applying FEA for designing a high efficiency 2.2 kW, 2p = 4 line start permanent magnet synchronous motor. In International Conference on Engineering Research and Applications, Cham: Springer Nature Switzerland, pp. 135-141. https://doi.org/10.1007/978-3-032-03856-2_15

[8] Le, A.T., Do, N.Y., Nguyen, T.K. (2025). Studying the effect of voltage unbalance on the working characteristics of LSPMSM. Journal Européen des Systèmes Automatisés, 58(1): 65-74. https://doi.org/10.18280/jesa.580108

[9] Jing, L., Gong, J., Lin, Y. (2019). Analysis and reduction of cogging torque of line-start permanent magnet motors. Progress in Electromagnetics Research M, 78: 115-124. https://doi.org/10.2528/PIERM18120902

[10] Behbahanifard, H., Sadoughi, A. (2016). Cogging torque reduction in line start permanent magnet synchronous motor. Journal of Electrical Engineering & Technology, 11(4): 878-888. http://doi.org/10.5370/JEET.2016.11.4.878

[11] Duc, H.B., Dinh, B.M., Bao, D.T., Tu, P.M., Vuong, D.Q. (2023). Improving performances of interior permanent magnet synchronous motors by using different rotor angles. Journal Européen des Systèmes Automatisés, 56(1): 115-120. https://doi.org/10.18280/jesa.560115

[12] Wan, X., Yang, S., Li, Y., Shi, Y., Lou, J. (2022). Minimization of cogging torque for V-type IPMSM by the asymmetric auxiliary slots on the rotor. IEEE Access, 10: 89428-89436. https://doi.org/10.1109/ACCESS.2022.3201246

[13] Sumega, M., Rafajdus, P., Scelba, G., Stulrajter, M. (2019). Control strategies for the identification and reduction of cogging torque in PM motors. In 2019 International Conference on Electrical Drives & Power Electronics (EDPE), the High Tatras, Slovakia, pp. 74-80. https://doi.org/10.1109/EDPE.2019.8883892

[14] Pierpaolo, D., Saponara, S. (2019). Control system design for cogging torque reduction based on sensor-less architecture. In International Conference on Applications in Electronics Pervading Industry, Environment and Society, Cham: Springer International Publishing, pp. 309-321. https://doi.org/10.1007/978-3-030-37277-4_36

[15] Petro, V., Kyslan, K., Horváth, K., Wróbel, K., Tarchała, G. (2025). HF pulse signal injection based method for sensorless control of PMSM with cogging torque compensation. In 2025 7th Global Power, Energy and Communication Conference (GPECOM), Bochum, Germany, pp. 257-262. https://doi.org/10.1109/GPECOM65896.2025.11061829
[16] Chu, H., Gao, B., Gu, W., Chen, H. (2016). Low-speed control for permanent-magnet DC torque motor using observer-based nonlinear triple-step controller. IEEE Transactions on Industrial Electronics, 64(4): 3286-3296. https://doi.org/10.1109/TIE.2016.2598298
[17] Liu, J., Li, H., Deng, Y. (2017). Torque ripple minimization of PMSM based on robust ILC via adaptive sliding mode control. IEEE Transactions on Power Electronics, 33(4): 3655-3671. https://doi.org/10.1109/TPEL.2017.2711098
[18] Bianchini, C., Immovilli, F., Lorenzani, E., Bellini, A., Davoli, M. (2012). Review of design solutions for internal permanent-magnet machines cogging torque reduction. IEEE Transactions on Magnetics, 48(10): 2685-2693. https://doi.org/10.1109/TMAG.2012.2199509
[19] Kim, K.C. (2014). A novel method for minimization of cogging torque and torque ripple for interior permanent magnet synchronous motor. IEEE Transactions on Magnetics, 50(2): 793-796. https://doi.org/10.1109/TMAG.2013.2285234
[20] Simón-Sempere, V., Simón-Gómez, A., Burgos-Payán, M., Cerquides-Bueno, J.R. (2021). Optimisation of magnet shape for cogging torque reduction in axial-flux permanent-magnet motors. IEEE Transactions on Energy Conversion, 36(4): 2825-2838. https://doi.org/10.1109/TEC.2021.3068174
[21] Anuja, T.A., Doss, M.A.N., Senthilkumar, R., Rajesh, K.S., Brindha, R. (2022). Modification of pole pitch and pole arc in rotor magnets for cogging torque reduction in BLDC motor. IEEE Access, 10: 116709-116722. https://doi.org/10.1109/ACCESS.2022.3217233
[22] Nakano, M., Morita, Y., Matsunaga, T. (2015). Reduction of cogging torque due to production tolerances of rotor by using dummy slots placed partially in axial direction. IEEE Transactions on Industry Applications, 51(6): 4372-4382. https://doi.org/10.1109/TIA.2015.2443110
[23] Xia, C., Chen, Z., Shi, T., Wang, H. (2013). Cogging torque modeling and analyzing for surface-mounted permanent magnet machines with auxiliary slots. IEEE Transactions on Magnetics, 49(9): 5112-5123. https://doi.org/10.1109/TMAG.2013.2256921
[24] Hwang, M.H., Lee, H.S., Cha, H.R. (2018). Analysis of torque ripple and cogging torque reduction in electric vehicle traction platform applying rotor notched design. Energies, 11(11): 3053. https://doi.org/10.3390/en11113053
[25] Morimoto, S., Inoue, Y., Sanada, M. (2023). Reducing cogging torque with rotor surface notches in double-layered IPMSMs. IEEJ Journal of Industry Applications, 12(6): 1096-1103. https://doi.org/10.1541/ieejjia.23003377
[26] Zhao, J., Wang, J., Zhou, L., Huang, W., Ma, Y., Zhang, Z. (2019). Cogging torque reduction by stepped slot-opening shift for interior permanent magnet motors. In 2019 22nd International Conference on Electrical Machines and Systems (ICEMS), Harbin, China, pp. 1-4. https://doi.org/10.1109/ICEMS.2019.8921448
[27] Patel, A.N. (2023). Slot opening displacement technique for cogging torque reduction of axial flux brushless DC motor for electric two-wheeler application. Electrical Engineering & Electromechanics, (2): 7-13. https://doi.org/10.20998/2074-272X.2023.2.02
[28] Jiang, J.W., Bilgin, B., Yang, Y., Sathyan, A., Dadkhah, H., Emadi, A. (2016). Rotor skew pattern design and optimisation for cogging torque reduction. IET Electrical Systems in Transportation, 6(2): 126-135. https://doi.org/10.1049/iet-est.2015.0021
[29] Hao, W., Wang, Y. (2018). Comparison of the stator step skewed structures for cogging force reduction of linear flux switching permanent magnet machines. Energies, 11(8): 2172. https://doi.org/10.3390/en11082172
[30] Stamenkovic, I., Jovanovic, D., Vukosavic, S. (2005). Torque ripple verification in PM machines. In EUROCON 2005-The International Conference on "Computer as a Tool", Belgrade, Serbia, pp. 1497-1500. https://doi.org/10.1109/EURCON.2005.1630248
[31] Studer, C., Keyhani, A., Sebastian, T., Murthy, S.K. (1997). Study of cogging torque in permanent magnet machines. In IAS'97, Conference Record of the 1997 IEEE Industry Applications Conference Thirty-Second IAS Annual Meeting, New Orleans, LA, USA, pp. 42-49. https://doi.org/10.1109/IAS.1997.643006
[32] Tsunata, R., Takemoto, M. (2024). Skewing technology for permanent magnet synchronous motors: A comprehensive review and recent trends. IEEE Open Journal of the Industrial Electronics Society, 5: 1251-1273. https://doi.org/10.1109/OJIES.2024.3491295
[33] Kim, B.T., Kim, D.K., Kwon, B.I., Lipo, T.A. (2008). Optimal skew angle for improving of start-up performance of a single-phase line-start permanent magnet motor. In 2008 IEEE Industry Applications Society Annual Meeting, Edmonton, AB, Canada, pp. 1-6. https://doi.org/10.1109/08IAS.2008.60
[34] Jagiela, M., Mendrela, E.A., Gottipati, P. (2013). Investigation on a choice of stator slot skew angle in brushless PM machines. Electrical Engineering, 95(3): 209-219. https://doi.org/10.1007/s00202-012-0252-8
[35] Tuan L.A., Nhu D.Y., Khanh N.T. (2026). Effect of phase angle unbalance on working characteristics of LSPMSM during transient process. International Journal of Engineering, 39(2): 454-464. https://doi.org/10.5829/ije.2026.39.02b.13